


RESEARCH ARTICLE

Comparison of ion transport determinants between a TMEM16 chloride channel and phospholipid scramblase

Dung M. Nguyen¹, Louisa S. Chen², Wei-Ping Yu², and Tsung-Yu Chen^{2,3} 

Two TMEM16 family members, TMEM16A and TMEM16F, have different ion transport properties. Upon activation by intracellular Ca^{2+} , TMEM16A—a Ca^{2+} -activated Cl^- channel—is more selective for anions than cations, whereas TMEM16F—a phospholipid scramblase—appears to transport both cations and anions. Under saturating Ca^{2+} conditions, the current-voltage (I-V) relationships of these two proteins also differ; the I-V curve of TMEM16A is linear, while that of TMEM16F is outwardly rectifying. We previously found that mutating a positively charged lysine residue (K584) in the ion transport pathway to glutamine converted the linear I-V curve of TMEM16A to an outwardly rectifying curve. Interestingly, the corresponding residue in the outwardly rectifying TMEM16F is also a glutamine (Q559). Here, we examine the ion transport functions of TMEM16 molecules and compare the roles of K584 of TMEM16A and Q559 of TMEM16F in controlling the rectification of their respective I-V curves. We find that rectification of TMEM16A is regulated electrostatically by the side-chain charge on the residue at position 584, whereas the charge on residue 559 in TMEM16F has little effect. Unexpectedly, mutation of Q559 to aromatic amino acid residues significantly alters outward rectification in TMEM16F. These same mutants show reduced Ca^{2+} -induced current rundown (or desensitization) compared with wild-type TMEM16F. A mutant that removes the rundown of TMEM16F could facilitate the study of ion transport mechanisms in this phospholipid scramblase in the same way that a CLC-0 mutant in which inactivation (or closure of the slow gate) is suppressed was used in our previous studies.

Introduction

The TMEM16 family of transmembrane proteins consists of Ca^{2+} -activated ion channels, such as TMEM16A and TMEM16B, and phospholipid scramblases, such as TMEM16F (Whitlock and Hartzell, 2017; Falzone et al., 2018). TMEM16A (Caputo et al., 2008; Schroeder et al., 2008; Yang et al., 2008) and TMEM16B (Stephan et al., 2009; Stöhr et al., 2009) control Cl^- transport across cell membranes and thus play important physiological roles in various functions, such as transepithelial fluid transport, intestinal smooth muscle contraction, and signal transduction in sensory neurons (Hartzell et al., 2005). The physiological role of TMEM16F, on the other hand, is different. After its activation by Ca^{2+} , TMEM16F scrambles phospholipids in the lipid membrane, resulting in the exposure of phospholipids normally residing in the inner leaflet of cell membranes (such as phosphatidylserine) to the extracellular environment (Suzuki et al., 2010, 2013; Yu et al., 2015), a process critical for many physiological functions (Bevers and Williamson, 2016; Whitlock and Hartzell, 2017). For example, the presence of phosphatidylserine in the outer leaflet of platelet cell membranes attracts blood coagulation factors to

the surface of platelet cells, thus facilitating the blood coagulation process. A defective function of TMEM16F, therefore, can cause a bleeding disorder called Scott syndrome (Suzuki et al., 2010; Castoldi et al., 2011).

Recent x-ray crystallography and cryo-electron microscopy studies have revealed the atomic structures of TMEM16 molecules (Brunner et al., 2014; Dang et al., 2017; Paulino et al., 2017a,b). The x-ray structure of a fungus phospholipid scramblase, nhTMEM16, displays a dimeric structure formed by two identical subunits (Fig. 1 A, right panel). Within each subunit, transmembrane helices 3–7 form an open aqueduct (or groove), residing distantly from the molecule's twofold symmetry axis, and this aqueduct is thought to be the lipid transport pathway (Brunner et al., 2014). The cryo-electron microscopy structure of TMEM16A (Fig. 1 A, left panel) shows a similar molecular architecture to that of nhTMEM16, except that transmembrane helix 4 of TMEM16A (helix colored in green in Fig. 1 B) is more tilted and partially covers the aforementioned aqueduct structure (Dang et al., 2017; Paulino et al., 2017a,b). Consequently, the extracellu-

¹Graduate Group of Pharmacology and Toxicology, University of California, Davis, Davis, CA; ²Center for Neuroscience, University of California, Davis, Davis, CA; ³Department of Neurology, University of California, Davis, Davis, CA.

Correspondence to Tsung-Yu Chen: tycchen@ucdavis.edu.

© 2019 Chen et al. This article is distributed under the terms of an Attribution–Noncommercial–Share Alike–No Mirror Sites license for the first six months after the publication date (see <http://www.rupress.org/terms/>). After six months it is available under a Creative Commons License (Attribution–Noncommercial–Share Alike 4.0 International license, as described at <https://creativecommons.org/licenses/by-nc-sa/4.0/>).

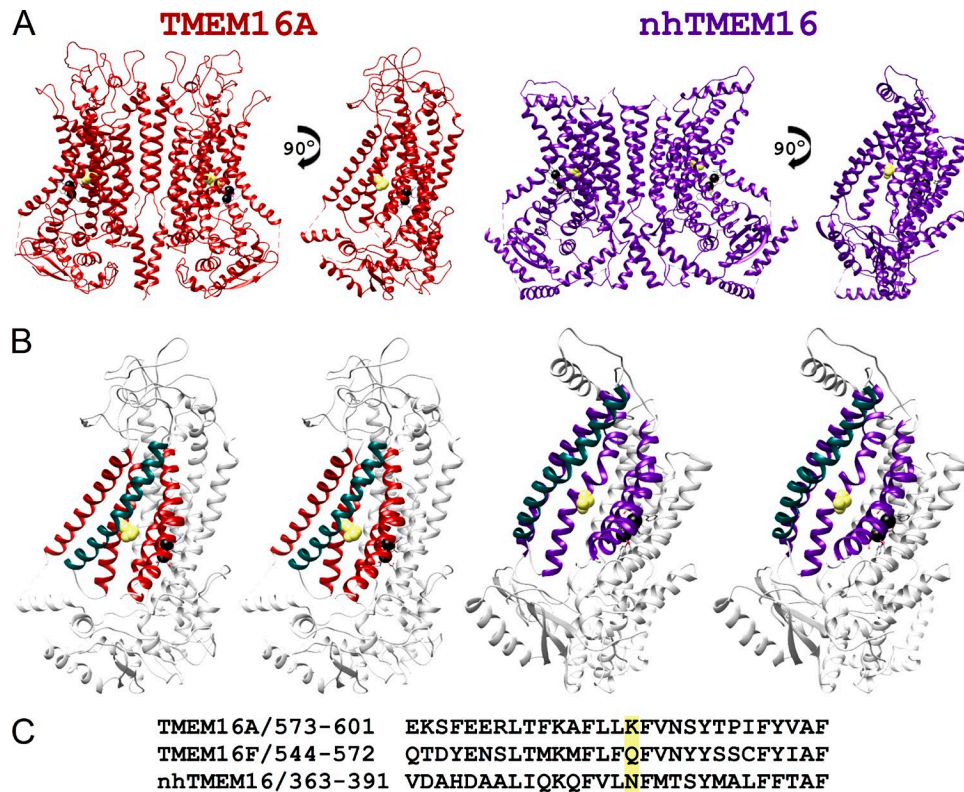


Figure 1. Atomic structures of TMEM16 proteins. (A) Structures of TMEM16A (red) and nhTMEM16 (purple). In each structure, the right subunit of the molecule rotated by 90° along the twofold symmetry axis is depicted on the right. Black spheres represent Ca²⁺ ions. (B) Stereo views of single TMEM16A (left) and nhTMEM16 (right) subunits highlighting the arrangement of helices 3–7. The view angle is the same as that of viewing the single subunit in A. Helix 3 and helices 5–7 of TMEM16A and TMEM16F are colored in red and purple, respectively, while helix 4 is in green in both molecules. (C) Sequence alignment of helix 5 of TMEM16A, TMEM16F, and nhTMEM16. K584_{16A}}, Q559_{16F}} and the corresponding residue N378 in nhTMEM16 (highlighted in yellow) are located in this helix. K584_{16A}} and N378 of nhTMEM16 are also depicted as a space-filled residue (colored in yellow) in the structures shown in A and B.

lar half of the aqueduct in TMEM16A is completely enclosed by helices 3–7 (compare the left and right panels in Fig. 1 B), forming a pore-like structure. Experimental evidence has suggested that this pore-like structure in TMEM16A is likely the pathway that conducts the current carried by Cl[−] (Jeng et al., 2016; Lim et al., 2016; Dang et al., 2017; Paulino et al., 2017b). Meanwhile, Ca²⁺-activated TMEM16F molecules also conduct ionic currents in addition to the phospholipid scramblase activity (Scudieri et al., 2015; Yu et al., 2015). It has been suggested that ion transport and phospholipid transport in TMEM16F share the same pathway (Yu et al., 2015; Jiang et al., 2017). However, while an aqueduct with the sidewall open can transport lipid molecules via a “credit card” sliding mechanism (Whitlock and Hartzell, 2017; Malvezzi et al., 2018), a structure without an enclosed protein conduit raises questions about the ion transport mechanism in phospholipid scramblases.

Although both TMEM16A and TMEM16F conduct currents upon activation by intracellular Ca²⁺ [Ca²⁺]_i, their selectivity of the transported ions differs. The pores of TMEM16A are more selective for anions (Ni et al., 2014; Jeng et al., 2016) while those of TMEM16F poorly discriminate cations from anions (Shimizu et al., 2013; Yu et al., 2015). In saturating [Ca²⁺]_i, the I–V curve of TMEM16A is quite linear, while that of TMEM16F is very outwardly rectifying (Shimizu et al., 2013; Yu et al., 2015). In structural–functional studies of TMEM16 molecules, functional roles

of pore residues have been examined (Yang et al., 2012; Jeng et al., 2016; Lim et al., 2016; Dang et al., 2017; Paulino et al., 2017a). In particular, one residue was thought to be critical for controlling the anion/cation selectivity in TMEM16A and TMEM16F (Yang et al., 2012). In TMEM16A, this pore residue is a positively charged lysine residue (K584, abbreviated as K584_{16A}}) in the alternatively spliced isoform “a” (or K588 in the “a, c” isoform), while it is a glutamine residue in TMEM16F (Q559_{16F}}). These corresponding residues are highlighted in the sequence alignment in Fig. 1 C, and their locations are depicted in Fig. 1, A and B, as a space-filled residue. It has been suggested that the positive charge from this residue in TMEM16A helps select anions over cations in TMEM16A, while the neutral residue in TMEM16F renders this phospholipid scramblase less selective for anions (Yang et al., 2012). In another aspect of ion transport function, we and others showed that mutating K584_{16A}} into glutamine (K584Q_{16A}}) generated a prominent outward rectification in the I–V curve of TMEM16A (Jeng et al., 2016; Lim et al., 2016).

The role of Q559_{16F}} in regulating the I–V curve rectification of TMEM16F has not been rigorously examined, although the Q559K_{16F}} mutant was shown to remain outwardly rectifying (Yang et al., 2012). In this study, we compared the residues K584_{16A}} and Q559_{16F}} in controlling the rectification of their respective I–V curves. We found that the side-chain charge of amino acid at position 584 of TMEM16A appears to control the

rectification of TMEM16A's I-V curve electrostatically. However, charge manipulation of residue 559 of TMEM16F was not consistent with an electrostatic regulation. Instead, we discovered that placing aromatic amino acids at position 559 of TMEM16F significantly reduced the outward rectification in this phospholipid scramblase. Furthermore, mutating Q559_{16F} into an aromatic amino acid also greatly reduced the rundown of TMEM16F current. We thus took advantage of the mutant with a more linear I-V curve and less current rundown to evaluate the properties of ion transport in TMEM16F.

Materials and methods

Molecular biology and channel expression

The alternatively spliced isoform “a” of the WT mouse TMEM16A cDNA (available from GenBank under accession no. NM_001242349.1) was a gift from L.Y. Jan (University of California, San Francisco, San Francisco, CA). We also obtained from Addgene the WT mouse TMEM16F tagged with mCherry on the C terminus (Addgene plasmid #62554), initially deposited by Han Renzhi (Loyola University Chicago Health Science Division, Maywood, IL). The WT TMEM16A (abbreviated as WT_{16A}) and the mCherry-removed WT TMEM16F (WT_{16F}) cDNAs, as well as their mutant cDNA constructs, were subcloned in pEGFP-N3 or pIRES2 expression vectors (Takara Bio). Mutations of cDNAs were made using the QuikChange II site-directed mutagenesis kit (Agilent Technologies) and were verified by commercial DNA sequencing services. These cDNA constructs produced channels with a GFP attached to the C terminus of the channel proteins (from pEGFP-N3 constructs) or channels without a GFP tag, but with a separate GFP protein (from pIRES2 constructs). The functional properties of these two types of constructs were indistinguishable. In this study, we used the GFP-tagged construct in all TMEM16A experiments. For the TMEM16F experiments, the dose-response curve was obtained from the GFP-tagged molecule, while the I-V curves were obtained from the untagged TMEM16F. WT_{16A}, WT_{16F}, and all mutants were expressed in human embryonic kidney (HEK) 293 cells. Transfections of cDNAs to HEK 293 cells were performed using the lipofectamine transfection method (Yu et al., 2014b; Jeng et al., 2016). Transfected cells were identified by the green fluorescence under an inverted microscope (DM IRB; Leica) equipped with a fluorescent light source and a GFP filter cube (Chroma Technology).

Electrophysiological experiments

All experiments were excised inside-out patch recordings and were conducted 24–72 h after transfections. The pipette solution contained 140 mM NaCl, 10 mM HEPES, and 0.1 mM EGTA at pH 7.4 (adjusted with NaOH). This solution, which will also be called “Solution A,” was considered to have nominally “zero” free [Ca²⁺]. Solutions containing various free [Ca²⁺] were made by adding CaCl₂ to Solution A followed by adjusting the pH. The required amounts of total Ca²⁺ for generating specific free [Ca²⁺] were calculated using the MaxChelator program (Bers et al., 2010), if the desired free [Ca²⁺] ≤ 10 μM. In experiments where various intracellular pH (pH_i) values (5.4–8.4) were necessary, the NaOH was also used to adjust the pH. For solutions containing

free [Ca²⁺] ≥ 20 μM, the total [Ca²⁺] added to Solution A was equal to the desired free [Ca²⁺] plus 0.1 mM. If the total added [CaCl₂] was >0.5 mM, [NaCl] was reduced accordingly to maintain a total [Cl⁻] at 140 mM. Free [Ca²⁺] in the intracellular side of excised inside-out patches will be abbreviated as [Ca²⁺]_i. In all experiments, the recording pipettes were made from borosilicate glass capillaries (World Precision Instruments) using the PP830 electrode puller (Narishige), and the electrode resistance was between ~1.5 and ~3.0 MΩ when filled with Solution A. All experiments were conducted using an Axopatch 200B amplifier, and the signals, filtered at 1 kHz, were digitized at 2 kHz by the Digidata analogue/digital signal-converting board controlled by the pClamp software (Molecular Devices). Solutions were delivered to the intracellular side of the excised inside-out patch using the SF-77 solution exchanger (Warner Instruments), which can switch solutions within a few milliseconds (Zhang and Chen, 2009).

To construct [Ca²⁺]-dependent activation curves, we used the previously described three-pulse protocol to minimize Ca²⁺-induced current rundown. The apparent Ca²⁺ affinity of activating TMEM16F was significantly lower than that of activating TMEM16A, so we used 900 μM [Ca²⁺]_i as the saturating [Ca²⁺]_i. The experimental protocol included a direct delivery to the cytoplasmic side of the membrane of 900 μM [Ca²⁺]_i, a test [Ca²⁺]_i (1–500 μM [Ca²⁺]_i), and finally 900 μM [Ca²⁺]_i again. The leak current, measured in the zero Ca²⁺ solution (Solution A), was subtracted from the current in the presence of Ca²⁺. The current activated by the test [Ca²⁺]_i pulse was normalized to the average of the two flanking saturating currents obtained in 900 μM [Ca²⁺]_i. For the dose-response activation curve of Q559W_{16F} and other aromatic mutants of TMEM16F, the three-pulse protocol described above was also employed. Due to these mutants' resistance to rundown, current activated with 0.1–1 mM [Ca²⁺]_i was normalized to current activated with 2 mM [Ca²⁺]_i instead of 900 μM [Ca²⁺]_i. With Q559W_{16F}, we also used another protocol to construct a dose-response curve, in which we sequentially applied various [Ca²⁺]_i, and normalized the Ca²⁺-induced current to the current activated by the maximal [Ca²⁺]_i. The purpose of using this latter protocol was to compare the results with those reported in the literature obtained with similar methods. In both types of experiments, normalized values of the Ca²⁺-induced current (I_{norm}) were plotted against [Ca²⁺]_i to construct dose-response curves.

I-V curves were constructed using a 1.6-s voltage ramp from –80 mV to +80 mV applied to the excised inside-out patches. For each patch, the recordings in Ca²⁺ free intracellular solutions were subtracted from that obtained in the presence of [Ca²⁺]_i, and the resulting leak-subtracted I-V curves were used to determine the reversal potential (E_{rev}). To average I-V curves from different membrane patches, the digitized data points from the ramp protocol were normalized to the last digitized point obtained at +80 mV, and the normalized values from different patches were averaged. All TMEM16A constructs were activated with 20 μM or 20 mM [Ca²⁺]_i. Additional I-V curves for WT_{16A} and K584H_{16A} were measured at pH 5.4, 6.4, and 7.4 with 400 μM [Ca²⁺]_i. All TMEM16F constructs were activated with 1 mM [Ca²⁺]_i. Additional I-V curves for Q559H_{16F} were constructed at pH 6.4, 7.4, and 8.4. To evaluate the degree of the I-V curve rectification, we

defined a parameter called the rectification index (RI), which is the ratio of the absolute current amplitudes at -80 mV versus that at $+80$ mV ($RI = |I_{-80\text{mV}}/I_{+80\text{mV}}|$). Thus, positive or negative deviation in RI from 1 indicates inward or outward rectification, respectively.

To measure E_{rev} under reduced NaCl conditions, the extracellular solution was Solution A, containing 140 mM NaCl. The intracellular NaCl concentration ($[\text{NaCl}]_i$) was made by mixing the 140 mM NaCl solution with the same concentration of (NMDG) $_2$ SO $_4$ solution, both containing identical [HEPES], [EGTA], $[\text{Ca}^{2+}\text{-EGTA}]$, and free $[\text{Ca}^{2+}]$ (Jeng et al., 2016). I-V curves of WT $_{16A}$, K584Q $_{16A}$, WT $_{16F}$ and Q559W $_{16F}$ were measured in the presence of various intracellular solutions containing 100% (~ 140 mM $[\text{NaCl}]_i$), 60% (~ 84 mM $[\text{NaCl}]_i$), or 30% (~ 42 mM $[\text{NaCl}]_i$) of Solution A, whereas the reduced $[\text{NaCl}]_i$ was replaced with the same concentration of (NMDG) $_2$ SO $_4$ solution. We also conducted the same experiments without adding (NMDG) $_2$ SO $_4$ to replace the reduced $[\text{NaCl}]_i$. To estimate the anion permeability sequence, E_{rev} was measured under bi-ionic conditions: $[\text{NaCl}]_i$ was replaced with identical concentrations of NaI or NaSCN. The liquid junction potentials in these various experiments were less than 2 mV except when reducing $[\text{NaCl}]_i$ without adding (NMDG) $_2$ SO $_4$. In experiments without adding (NMDG) $_2$ SO $_4$, the junction potentials were 2.6 mV and 6 mV for 84 mM and 42 mM $[\text{NaCl}]_i$, respectively. All the reported E_{rev} values have been corrected for liquid junction potentials.

To alter the charge of the introduced cysteine residue, we used methanethiosulfonate (MTS) reagents to modify the free thiol group of the cysteine side chain. MTS reagents such as sulfonatoethyl MTS (MTSES) and ethyltrimethylammonium MTS (MTSET) were purchased from Toronto Research Chemicals. High concentrations of MTS reagents were made in double-distilled H $_2$ O and were stored at -80°C . Upon use, stock solutions of MTS reagents were thawed and placed on ice and were directly diluted into the working solution. To modify the channels in excised inside-out patches, WT $_{16A}$ and K584C $_{16A}$ were activated with 20 μM $[\text{Ca}^{2+}]_i$ at -40 mV before the application of MTS reagents. I-V curves of the channels before and after MTS modification were obtained as previously described.

Data analysis

Experimental data were analyzed using Clampfit 10 software (Molecular Devices) and Origin software (OriginLab).

To evaluate the apparent Ca^{2+} affinity for activating TMEM16 molecules, data points of the normalized current (I_{norm}) in the dose-response plot were fitted to the Hill equation

$$I_{\text{norm}} = 1 / \{1 + (K_{1/2} / [\text{Ca}^{2+}]_i)^h\},$$

where $K_{1/2}$ and h are the fitted half-effective concentration and the Hill coefficient, respectively.

Permeability ratios of Na $^+$ versus Cl $^-$ ($P_{\text{Na}}/P_{\text{Cl}}$) were calculated according to the Goldman-Hodgkin-Katz equation

$$E_{\text{rev}} = (RT/F) \ln \left(\frac{P_{\text{Na}}[\text{Na}^+]_o + P_{\text{Cl}}[\text{Cl}^-]_i}{P_{\text{Na}}[\text{Na}^+]_i + P_{\text{Cl}}[\text{Cl}^-]_o} \right)$$

where R , T , and F are the ideal gas constant, absolute temperature, and Faraday constant, respectively.

All averaged data are presented as means \pm SEM. Student's t test was used for statistical comparisons among the datasets of fixed-charge mutations. For MTS modification experiments, a paired Student's t test was employed to compare the datasets before and after 12-s MTS modifications. Differences were considered statistically significant if $P < 0.05$.

Online supplemental material

Fig. S1 shows MTSET modification effects of K584C $_{16A}$ after pre-exposing the mutant channels to MTSES intracellularly.

Results

Roles of K584 $_{16A}$ in the rectification of TMEM16A's I-V curve

TMEM16A is a dimeric Cl $^-$ channel (Fallah et al., 2010; Sheridan et al., 2011; Tien et al., 2013) with two distinct pores. The two-pore architecture was first suggested based on the observations that mutating K584 $_{16A}$ (or K588 $_{16A}$ of the "a, c" isoform of TMEM16A) into a neutral residue, glutamine, generated an outwardly rectifying I-V curve, and that this mutation effect was subunit specific (Jeng et al., 2016; Lim et al., 2016). The high-resolution structure of TMEM16A confirms the location of this positively charged residue in the pore (Dang et al., 2017; Paulino et al., 2017a,b). Therefore, TMEM16A's I-V curve rectification, caused by the K584Q $_{16A}$ mutation, might reflect an electrostatic effect of losing a positive charge on Cl $^-$ conduction. Such an electrostatic control has been documented in CLC-0, in which the mutation of K519 of this *Torpedo* Cl $^-$ channel can alter the anion permeation electrostatically (Middleton et al., 1996; Chen and Chen, 2003). A recent study also showed that Ca^{2+} binding to the binding sites of TMEM16A, which are close to the location of K584 $_{16A}$, can electrostatically influence anion permeation in the pore (Lam and Dutzler, 2018). To verify this possibility, we mutated K584 $_{16A}$ into amino acids with different side-chain charges. Fig. 2A shows that placing any neutral amino acids at this position caused a significant outward rectification of the I-V curve obtained in saturating $[\text{Ca}^{2+}]_i$ with symmetrical 140 mM $[\text{Cl}^-]$. When a negatively charged residue, such as glutamate or aspartate, was introduced at this position, the I-V curves were even more outwardly rectifying. On the other hand, introducing a positively charged residue at this position, i.e., the K584R $_{16A}$ mutation, only affected the rectification slightly. To compare the degree of rectification, we defined the RI as the ratio of the absolute value of the current at -80 mV to that at $+80$ mV. The mutation experiments revealed that the value of the RI followed with the side-chain charge of the residue 584: mutants with a negatively charged side chain had the smallest RI, while those with the positively charged residues had the largest RI. However, since the I-V curve of the WT $_{16A}$ exhibits outward rectification in nonsaturating $[\text{Ca}^{2+}]_i$ (Kuruma and Hartzell, 2000; Yang et al., 2008; Yu et al., 2012), we also conducted the experiments with 20 mM $[\text{Ca}^{2+}]_i$ to ensure maximum activation of all TMEM16A mutants. As shown in Fig. 2B, the pattern of the electrostatic influence on RI is preserved for I-V curves obtained at 20 mM $[\text{Ca}^{2+}]_i$.

To examine the electrostatic control of ion transport in TMEM16A more rigorously, we adopted two other methods to alter the side-chain charge of residue 584. First, we placed histi-

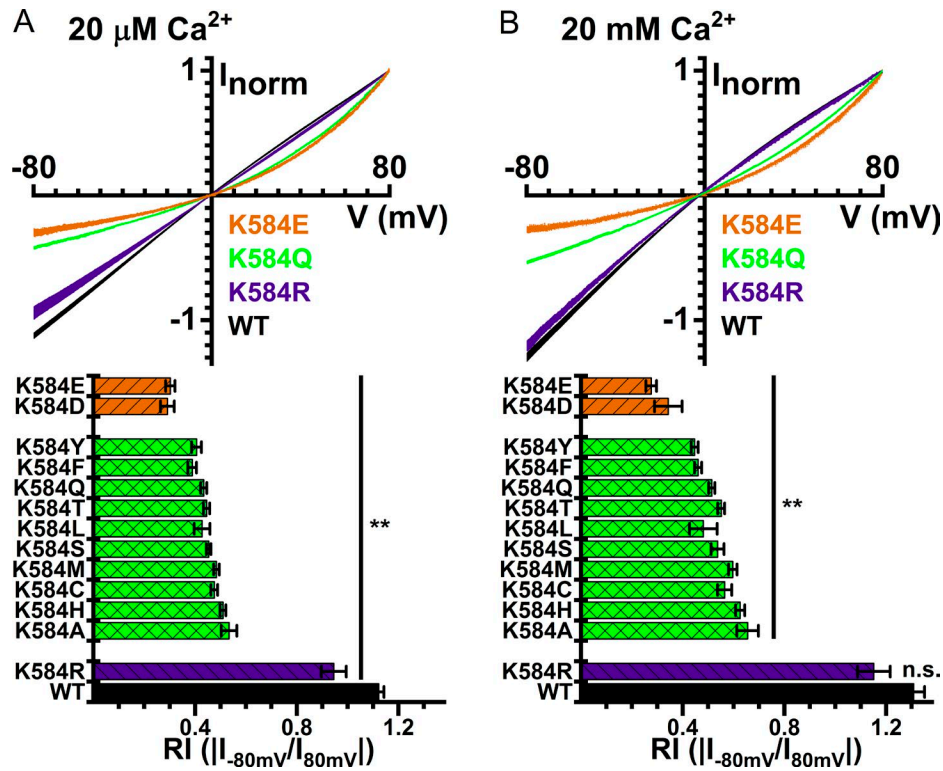


Figure 2. I-V curves of WT TMEM16A and mutants. I-V curves in the presence of (A) 20 μM and (B) 20 mM [Ca²⁺]_i. Symmetrical 140 mM [Cl⁻]_i. In both A and B, averaged I-V curves of WT_{16A}, K584Q_{16A}, K584R_{16A}, and K584E_{16A} are depicted on top, while the averaged RI values (means ± SEM, n = 3–36) of the WT_{16A} and various mutants are shown at the bottom. **, P < 0.005 by Student's t test compared with WT_{16A}. n.s., not significant.

dine at this position (K584H_{16A}) and measured the effect of pH_i on the I-V curve (Chen and Chen, 2003). Lowering pH_i, however, may reduce the channel affinity for Ca²⁺ because the Ca²⁺-binding site of TMEM16A consists of several acidic residues such as E698, E701, E730, and D734 (Yu et al., 2012; Brunner et al., 2014; Tien et al., 2014; Dang et al., 2017; Paulino et al., 2017a). The I-V curve of TMEM16A in nonsaturating [Ca²⁺]_i is known to be outwardly rectifying, which could complicate the interpretation of the results. Therefore, we used a higher [Ca²⁺]_i (400 μM) to activate the current in this experiment. Lowering the pH_i does not cause a decrease of RI in WT_{16A} (Fig. 3 A), indicating that 400 μM [Ca²⁺]_i is high enough to fully open the channel even at lower pH_i conditions. For K584H_{16A}, a reduction of pH_i from 7.4 to 5.4 incrementally increases the RI value in K584H_{16A} (Fig. 3 B), likely due to the more positively charged side chain of histidine. Another approach to alter the side-chain charge is to modify a cysteine residue at position 584 (K584C_{16A} mutation) with charged MTS reagents, such as MTSES or MTSET, which add a negative and a positive charge to the cysteine side chain, respectively (Middleton et al., 1996; Chen and Chen, 2003). The WT_{16A} channel contains endogenous cysteine residues. However, neither 10 mM MTSES nor 2 mM MTSET alters the Ca²⁺-activated current in WT_{16A} (Fig. 3, C and D, left panel). In contrast, MTSES and MTSET decrease and increase the current of K584C_{16A}, respectively (Fig. 3, C and D, middle panel), although the current alteration effect of MTSET appears to be larger. It is also worth noting that millimolar concentrations of MTS reagents are required to alter current within several seconds, so their modification rates of

K584C_{16A} are at least 30 times slower than the corresponding modifications of K519C of CLC-0 (Lin and Chen, 2003). The modification by 10 mM MTSES for 12 s renders the I-V curve more outwardly rectifying (Fig. 3 C, right), albeit the effect on the RI reduction is small. In contrast, MTSET modification generates a greater effect on altering the RI value, and the modification by 2 mM MTSET for 12 s generates a nearly linear I-V curve (Fig. 3 D, right), suggesting that such an MTSET exposure likely modifies most of the K584C_{16A} mutants. The smaller MTSES modification effect is consistent with the observation that the RI difference between constructs with a neutral and a negatively charged residue at position 584 is smaller than the difference between those with a neutral and a positively charged mutation (Fig. 2). In addition, exposing the membrane patch for the same duration to 10 mM MTSES, which has an intrinsic reactivity 12-fold lower than that of MTSET (Stauffer and Karlin, 1994), is not enough to fully modify all K584C_{16A} mutants. This is shown by separate experiments in which MTSET induces current in patches pre-exposed to 10 mM MTSES for 12 s, and thus increases RI (Fig. S1). Regardless of the slow MTS modification rates, the I-V curves become more outwardly rectifying in every individual patch after the application of 10 mM MTSES for 12 s (Fig. 3 C, right), whereas outward rectification was decreased after MTSET modification (Fig. 3 D, right). These MTS modification results and the pH titration effects shown above mimic those shown in CLC-0, where a positively charged residue, K519, electrostatically controls the efflux of Cl⁻ in the CLC-0 pore (Middleton et al., 1996; Chen and Chen, 2003).

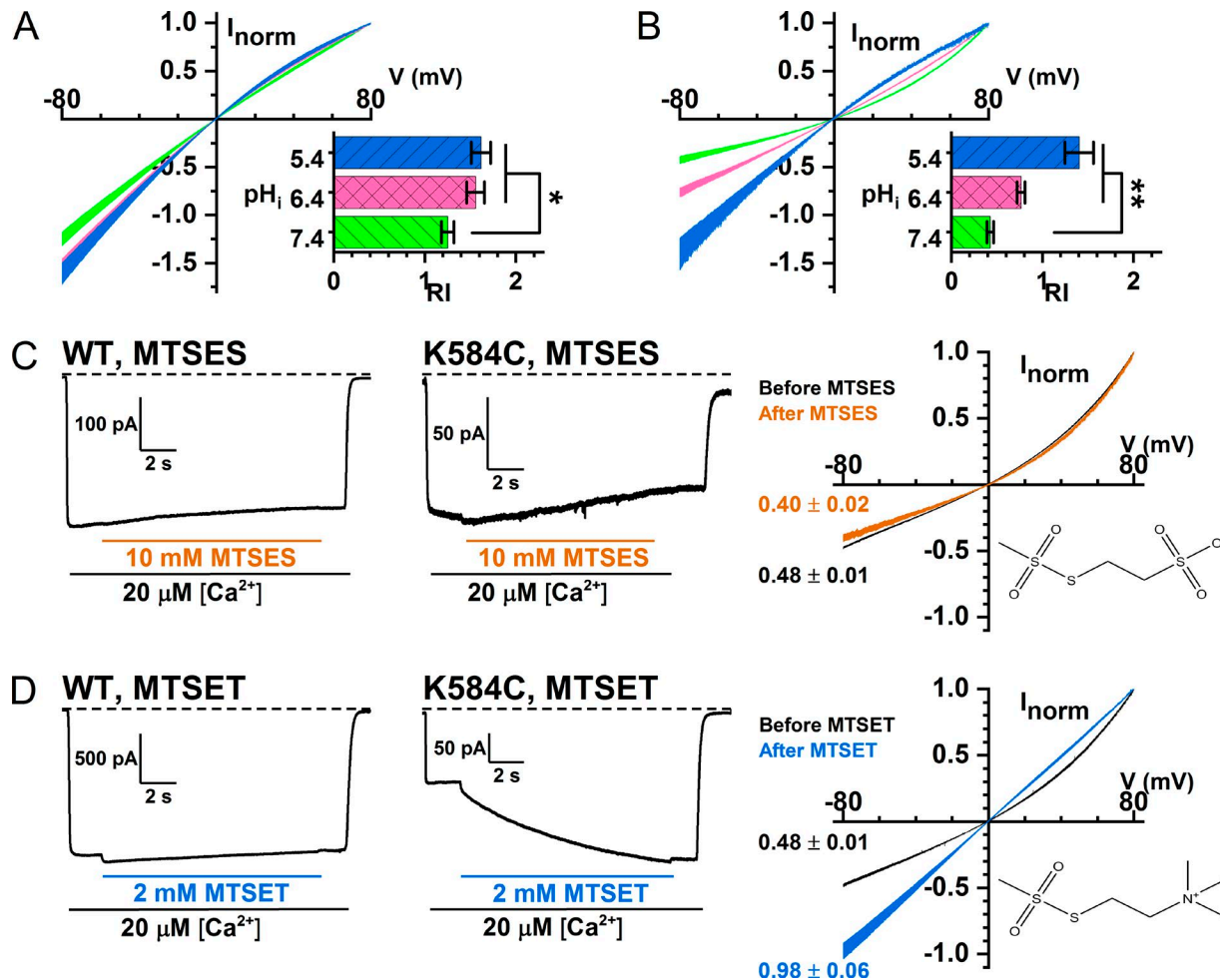


Figure 3. **Side-chain charge modifications of the residue at position 584 of TMEM16A.** (A and B) I-V curves of WT_{16A} (A) and K584H_{16A} (B) with 400 μM [Ca²⁺]_i at pH 5.4 (blue), 6.4 (pink), and 7.4 (green). Insets show averaged rectification indices ($n = 6$, *, $P < 0.05$ and **, $P < 0.005$ by Student's t test). (C and D) Manipulation of the side-chain charge of K584C_{16A} by MTSES (C) and MTSET (D) modifications. In each panel, recording traces of MTS modifications of WT_{16A} and K584C_{16A} at -40 mV are depicted on the left and middle, respectively. The dashed line represents zero current level. The structures of the MTS molecules and the I-V curves of K584C_{16A} before and after MTS modification are shown on the right. The RI values are displayed next to each I-V curve. The RI values after MTSES ($n = 9$) and MTSET ($n = 6$) modifications were significantly different from those before the modifications ($P < 0.05$, paired Student's t test).

Roles of Q559_{16F} in the rectification of TMEM16F's I-V curve

TMEM16F, a phospholipid scramblase in the TMEM16 family, can also conduct ionic current upon activation by [Ca²⁺]_i. We were thus curious whether the charge of residue 559 of TMEM16F also controls the rectification of its I-V curve. Before answering this question, we evaluated the apparent Ca²⁺ affinity of the WT_{16F} to determine a saturating [Ca²⁺]_i suitable for the experiments (Fig. 4 A). With excised inside-out patch recordings, the TMEM16F current appeared almost immediately upon the application of [Ca²⁺]_i, and the current induced by high [Ca²⁺]_i ran down quickly (Fig. 4 A). We thus constructed the [Ca²⁺]_i-dependent activation curve using the standard three-pulse methods and normalized the current in tested [Ca²⁺]_i to the mean of the saturated current (induced by 900 μM [Ca²⁺]_i) immediately before and after the tested [Ca²⁺]_i (Ni et al., 2014). Such a dose-response relationship shows that at +40 mV, the $K_{1/2}$ for Ca²⁺ was 34 μM and the Hill coefficient was 1.2 (Fig. 4 B). Since TMEM16F currents run down within several seconds, the dose-response curve in Fig. 4 B likely comes from the partially

rundown TMEM16F, which has a lower Ca²⁺ affinity than the pre-rundown TMEM16F (Ye et al., 2018). As the dose-response curve indicated that it requires more than ~100 μM [Ca²⁺]_i for a near saturation of Ca²⁺ activation, we obtained I-V curves at a 10-fold higher [Ca²⁺]_i (1 mM) to ensure full activation of TMEM16F. WT_{16F} contains a neutral residue (glutamine) at position 559, but mutating Q559_{16F} into charged amino acid residues did not drastically alter the rectification of its I-V curve: Q559E_{16F} and Q559D_{16F} mutations did not significantly alter the values of RI, while Q559R_{16F} and Q559K_{16F} mutations only caused a small increase in RI (Fig. 5, A and B). Furthermore, titrating the side-chain charge of Q559H_{16F} with pH_i generated a result inconsistent with an electrostatic control; lowering pH_i from 7.4 to 5.4 actually decreases RI in the Q559H_{16F} mutant (Fig. 5, C and D). Therefore, we conclude that there is no clear pattern of a significant electrostatic control of the I-V curve rectification by the charge from residue 559 in TMEM16F.

Among the various mutations of Q559_{16F}, we found unexpectedly that introducing an aromatic amino acid at position

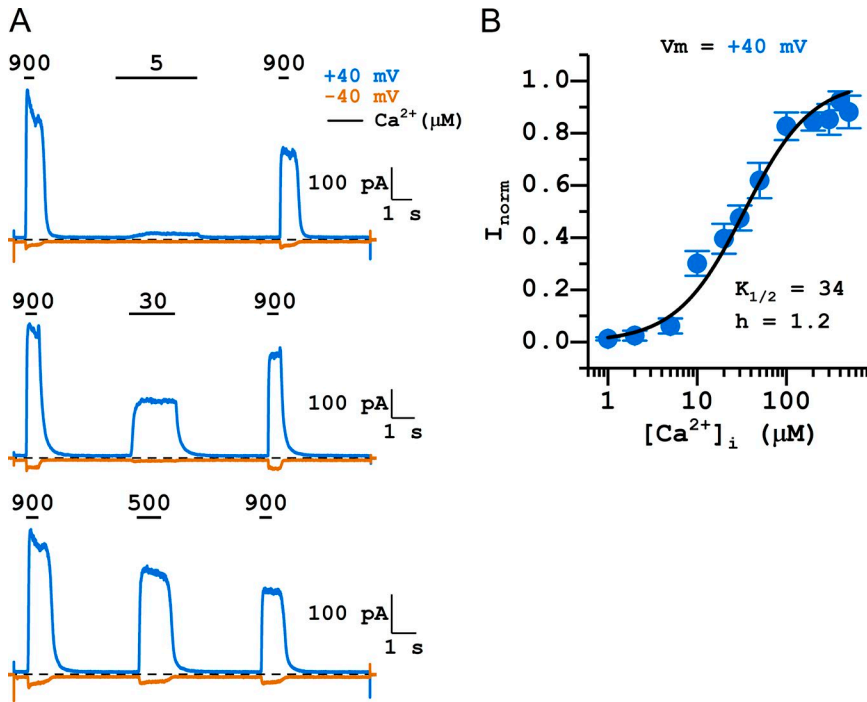


Figure 4. $[Ca^{2+}]_i$ -dependent activation of WT_{16F}. Symmetrical 140 mM $[Cl^-]$. (A) Representative traces obtained at +40 mV (blue) and -40 mV (orange) showing the three-pulse protocol. Dashed lines are zero current level. Numbers and horizontal bars on top of the traces indicate the application of indicated $[Ca^{2+}]_i$ (in micromolar). Notice the rapid current run-down of TMEM16F. (B) $[Ca^{2+}]_i$ -dependent activation curve of TMEM16F. All current was normalized to that obtained with 900 μM $[Ca^{2+}]_i$. Data points were the average of 3–12 independent measurements (mean \pm SEM). The fitted values of $K_{1/2}$ and Hill coefficient (h) are shown next to the fitted curve.

559 significantly reduces the I-V curve outward rectification. Fig. 5, A and B, shows that the I-V curves of Q559W_{16F}, Q559H_{16F}, Q559Y_{16F} and Q559F_{16F} all have significant increases in their RIs, which were 0.45 ± 0.03 ($n = 10$), 0.23 ± 0.03 ($n = 11$), $0.22 \pm$

0.04 ($n = 10$), and 0.19 ± 0.03 ($n = 9$), respectively. In comparison, the RI of WT_{16F} was 0.05 ± 0.01 ($n = 15$). Although other possibilities exist, the simplest interpretation for these findings is that the region near Q559_{16F}, like the corresponding region in

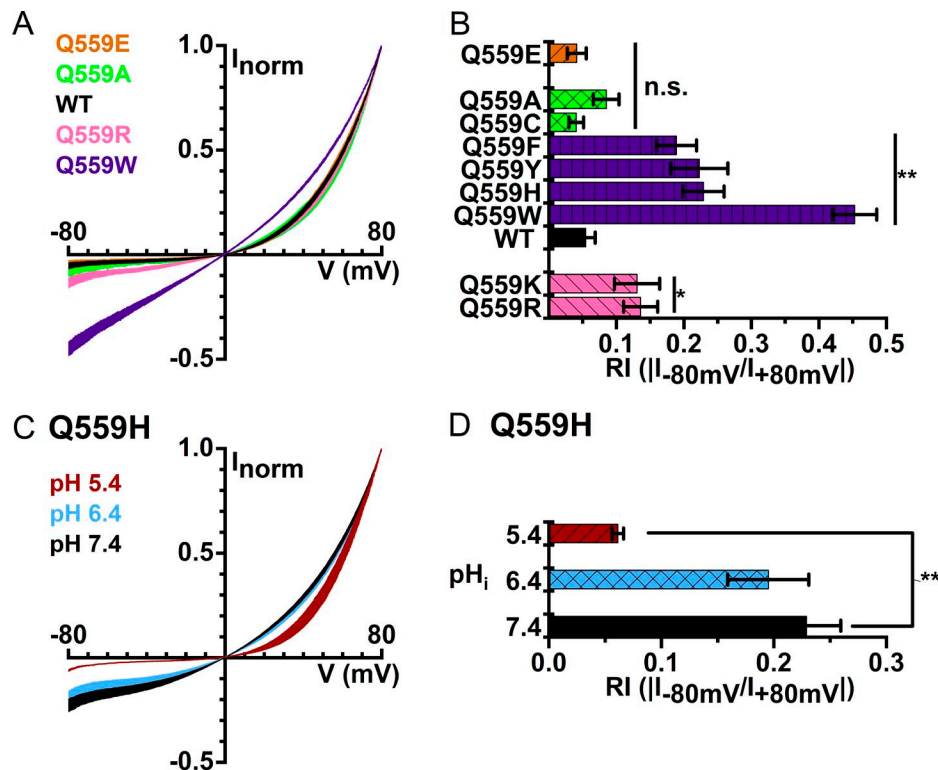


Figure 5. I-V curves of WT_{16F} and mutants in symmetrical 140 mM $[Cl^-]$ and with 1 mM $[Ca^{2+}]_i$. (A) Averaged I-V curves of Q559E_{16F} (orange), Q559A_{16F} (green), WT_{16F} (black), Q559R_{16F} (pink), and Q559W_{16F} (purple; $n = 4$ –11). (B) Rectification indices of WT_{16F} and various mutants. (C) I-V curves of Q559H_{16F} at pH_i 7.4 (black), 6.4 (blue), and 5.4 (red). (D) Averaged rectification indices of Q559H_{16F} at different pH_i. *, $P < 0.05$ and **, $P < 0.005$ by Student's *t* test compared with WT_{16F} at pH_i = 7.4.

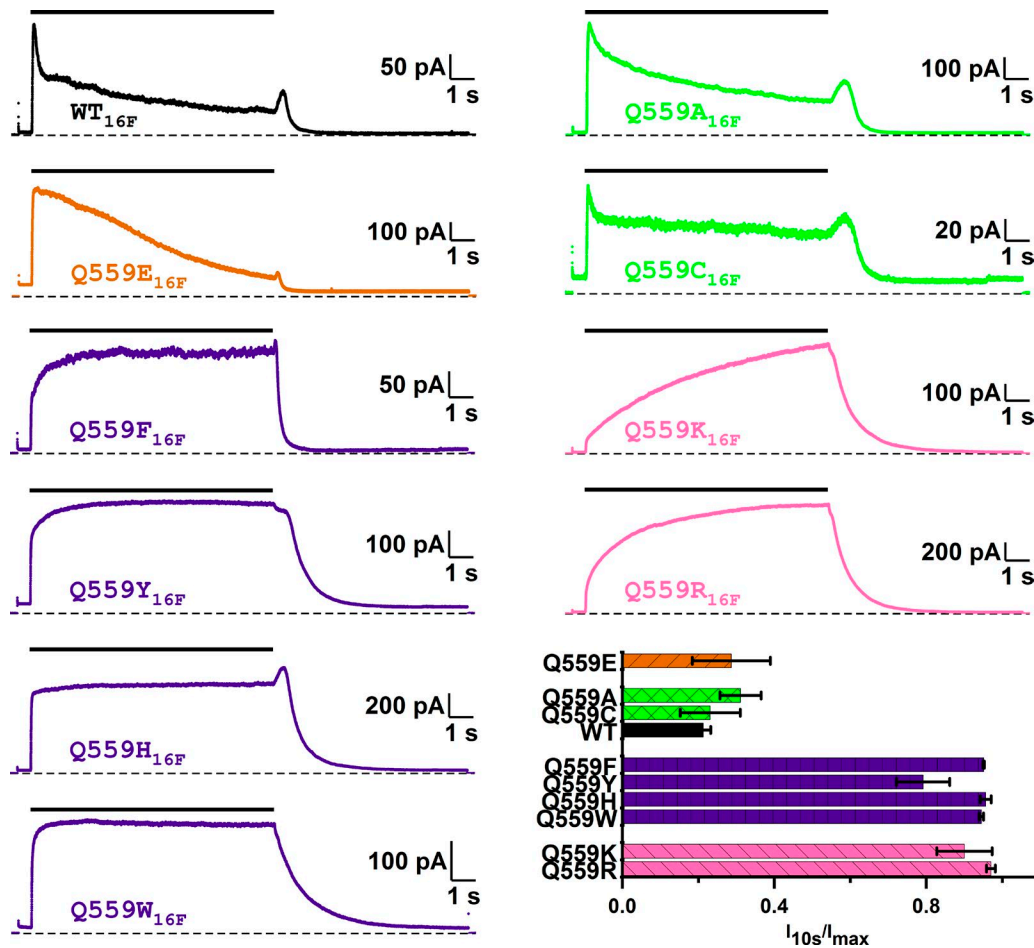


Figure 6. **Mutation of Q559_{16F} alters the Ca²⁺-dependent rundown of TMEM16F.** WT_{16F} (black) and various mutants of Q559_{16F} were activated by 2 mM [Ca²⁺]_i at +40 mV in symmetrical 140 mM [Cl⁻]. Dashed lines are zero current level. Black horizontal line segments above the traces indicate the 10-s application of 2 mM [Ca²⁺]_i. To evaluate the degree of Ca²⁺-induced rundown, the current measured at the end of the 10-s [Ca²⁺]_i exposure (I_{10s}) was divided by the maximal current (I_{max}) in the same 10-s recording in [Ca²⁺]_i. Bar graph shows the averaged values of I_{10s}/I_{max}, indicating the nondesensitized current fraction after exposure to 2 mM [Ca²⁺]_i for 10 s (n = 3–8).

TMEM16A, could be involved in the ion transport of this phospholipid scramblase.

Q559_{16F} is critical for the rundown of TMEM16F currents

The second interesting finding of placing an aromatic amino acid at position 559 of TMEM16F is that these mutants show little current rundown induced by high [Ca²⁺]_i. As shown in Fig. 6 (top trace), the WT TMEM16F current activated by 2 mM [Ca²⁺]_i runs down significantly within several seconds. On the other hand, Q559W_{16F}, Q559H_{16F}, Q559Y_{16F}, and Q559F_{16F} do not exhibit significant current rundown from the same [Ca²⁺]_i application (Fig. 6). For comparison, introducing neutral amino acids such as alanine and cysteine, or negatively charged amino acids such as glutamate, still maintains the quick rundown response. On the other hand, introducing positively charged amino acids does not cause rundown in the same high [Ca²⁺]_i. Instead, a slowly increased current upon [Ca²⁺]_i application was observed in Q559K_{16F} and Q559R_{16F} mutants. We also tested the rundown for a more prolonged time in Q559W_{16F} and found little rundown in this mutant, even with 2 mM [Ca²⁺]_i for 3 min (Fig. 7 A). These results reveal that residue 559 of TMEM16F is critical for controlling the rundown of TMEM16F.

The unexpected findings that the [Ca²⁺]_i-induced rundown in TMEM16F can be prevented and that the I-V curves are more linear in mutants with aromatic amino acids at position 559 provide an opportunity for more reliable assessment of the functional properties of TMEM16F. A more linear I-V curve allows a better estimate of the E_{rev}, while little current rundown makes the construction of [Ca²⁺]_i-dependent activation curve less prone to rundown-induced errors (Ni et al., 2014). We thus characterized the apparent Ca²⁺ affinity and ion permeability functions in these mutants. We employed two different protocols to construct [Ca²⁺]_i-dependent activation curves of Q559W_{16F} (Fig. 7, B and C). While the Hill coefficient of WT_{16F} and that of the Q559W_{16F} mutant are similar, the K_{1/2} of the dose-response activation curve in the Q559W_{16F} is significantly different from that of the WT_{16F} (Fig. 7), but similar to that of the pre-rundown WT_{16F} reported in the literature (Ye et al., 2018). Other mutants with an aromatic residue at position 559 also have apparent Ca²⁺ affinities similar to that of the pre-rundown WT_{16F} as well (Table 1). For Q559K_{16F} and Q559R_{16F}, although the current rundown was also suppressed, a slow continuous increase of the Ca²⁺-induced current generated a

Table 1. Ca²⁺-dependent activation of WT TMEM16F and aromatic Q559 mutants using the three-pulse protocol

Channel	Ca ²⁺ dose-response	
	K _{1/2} (μM)	Hill coefficient
WT _{16F} ^a	34 ± 3	1.2 ± 0.1
Q559F _{16F}	10 ± 1	1.5 ± 0.1
Q559Y _{16F}	7.9 ± 0.9	1.3 ± 0.1
Q559H _{16F}	3.2 ± 0.6	1.9 ± 0.2
Q559W _{16F}	2.2 ± 0.7	0.9 ± 0.2

^aChannel likely in partially rundown state.

technical uncertainty to determine the steady-state current. Therefore, we did not construct [Ca²⁺]_i-dependent activation curves for these two mutants.

The Q559W_{16F} mutation does not significantly alter ion permeation of TMEM16F

To further characterize the rundown-resistant TMEM16F mutants, we compared ion permeation functions between WT_{16A} and WT_{16F} in two aspects: the anion/cation selectivity, and the permeability of I⁻ and SCN⁻ relative to that of Cl⁻. The former was assessed by measuring the E_{rev} in reduced [NaCl]_i conditions: 60% (84 mM) and 30% (42 mM) of the extracellular [NaCl] (Fig. 8, A and B), while the latter was evaluated by experiments in which [Cl⁻]_i was replaced with equal concentrations of a different anion (Fig. 8, C and D). Unlike our previous results in WT_{16A} with the same ionic conditions (Jeng et al., 2016), reducing [NaCl]_i to 42 mM (30% of the control concentration) resulted in only a small shift of the E_{rev}. The values of E_{rev} were 0.7 ± 0.7 mV and 1.3 ± 0.8 mV for WT_{16F} and 2.8 ± 0.4 mV and 4.3 ± 0.9 mV for Q559W_{16F} in 84 mM and 42 mM [NaCl]_i, respectively (Fig. 8 B), in the experiments where the reduced [NaCl]_i was replaced with (NMDG)₂SO₄. Comparing these measured E_{rev} values with a perfect Cl⁻ Nernstian curve indicates that the pore of WT_{16F} does not selectively conduct Cl⁻, and the Q559W_{16F} mutation does not change this property (Fig. 8 B). Because the permeability of TMEM16F for the ions that replace [NaCl]_i (namely, NMDG⁺ and SO₄²⁻) were not certain, we further conducted similar experiments in reduced [NaCl]_i solutions without (NMDG)₂SO₄. The E_{rev} values were 1.7 ± 0.7 mV and 5.4 ± 1.8 mV for WT_{16F} and -0.2 ± 0.7 mV and -1.4 ± 2.9 mV for Q559W_{16F} in 84 mM and 42 mM [NaCl]_i, respectively (Fig. 8 B). The calculated P_{Na}/P_{Cl} permeability ratios were estimated to be ~1.3 and ~1.0 for WT_{16F} and Q559W_{16F}, respectively, based on the values of E_{rev} obtained with 84 mM [NaCl]_i.

The permeability of I⁻ and SCN⁻ relative to that of Cl⁻ was evaluated from bi-ionic experiments shown in Fig. 8 C. In both WT_{16F} and Q559W_{16F}, replacing [NaCl]_i with equal concentrations of [NaI]_i or [NaSCN]_i generated significant shifts of E_{rev} toward more positive potentials (~14 mV and ~25 mV, respectively; Fig. 8, C and D), suggesting that I⁻ and SCN⁻ are more permeable than Cl⁻ in TMEM16F. The shifts of E_{rev} in WT_{16F} and Q559W_{16F} were not statistically different, indicat-

ing that the Q559W_{16F} mutation did not alter the selectivity among these anions.

Discussion

TMEM16 family members play important roles in various physiological functions. TMEM16A participates in transmembrane Cl⁻ transport, while TMEM16F scrambles membrane phospholipids. Although ion transport across lipid membranes appears unnecessary for the known physiological role of TMEM16F, this protein also conducts ionic current upon activation by Ca²⁺. It has been shown that the scramblase activity and the current conduction of TMEM16F accompany each other, suggesting that ion transport in TMEM16F may be involved in the process of phospholipid transport (Yu et al., 2015). High-resolution structural studies show that the mouse TMEM16A molecule and the fungus phospholipid scramblase, nhTMEM16, adopt a similar structural architecture, including the conserved Ca²⁺-binding sites (Brunner et al., 2014; Dang et al., 2017; Paulino et al., 2017a,b). Nonetheless, the potential ion transport pathways appear to be slightly different between these two molecules. In TMEM16A, the extracellular half of the ion transport pathway is enclosed by several helices (see the left stereo pair in Fig. 1 B). On the other hand, the corresponding pathway in nhTMEM16 appears to be an open “aqueduct,” in which the sidewall of the entire pathway is open (right stereo pair in Fig. 1 B). To understand the ion transport mechanisms of TMEM16 members with or without an enclosed pore, we compared the functional properties between TMEM16A and TMEM16F. In excised inside-out patches, both molecules conducted ionic currents almost immediately after Ca²⁺ was applied to the intracellular side of the membrane, although a delayed current activation of TMEM16F was previously reported in whole-cell recording conditions (Grubb et al., 2013; Yu et al., 2015). An easily identified difference between the two molecules is that TMEM16A appears to be more sensitive to Ca²⁺ activation than TMEM16F. Only sub-micromolar [Ca²⁺]_i is required to open the pore of TMEM16A, while micromolar [Ca²⁺]_i is necessary to induce current in TMEM16F.

Roles of K584_{16A} and Q559_{16F} in the I-V curve rectification

Another difference between WT_{16A} and WT_{16F} is the rectification of their I-V curves. In symmetrical 140 mM [Cl⁻]_i with a saturated [Ca²⁺]_i, the I-V curve of WT_{16A} is linear (Fig. 2), while that of WT_{16F} is very outwardly rectifying (Fig. 5). Previous experiments have shown that when a positively charged residue, K584_{16A} (in the “a” alternatively spliced variant, corresponding to K588_{16A} in the “a, c” spliced variant), is mutated to glutamine, the linear I-V curve of WT_{16A} becomes outwardly rectifying in K584Q_{16A} (Jeng et al., 2016; Lim et al., 2016). Interestingly, WT_{16F}, which has an outwardly rectifying I-V curve, contains a glutamine residue at the corresponding position (Q559_{16F}). To understand the roles of K584_{16A} and Q559_{16F} in regulating the I-V curve rectification, we first examined if the outward rectification observed in K584Q_{16A} resulted from the removal of a positive charge. We mutated K584_{16A} into various amino acids and showed that the side-chain charge from the introduced residue correlated with the degree of outward rectification in TMEM16A: the more neg-

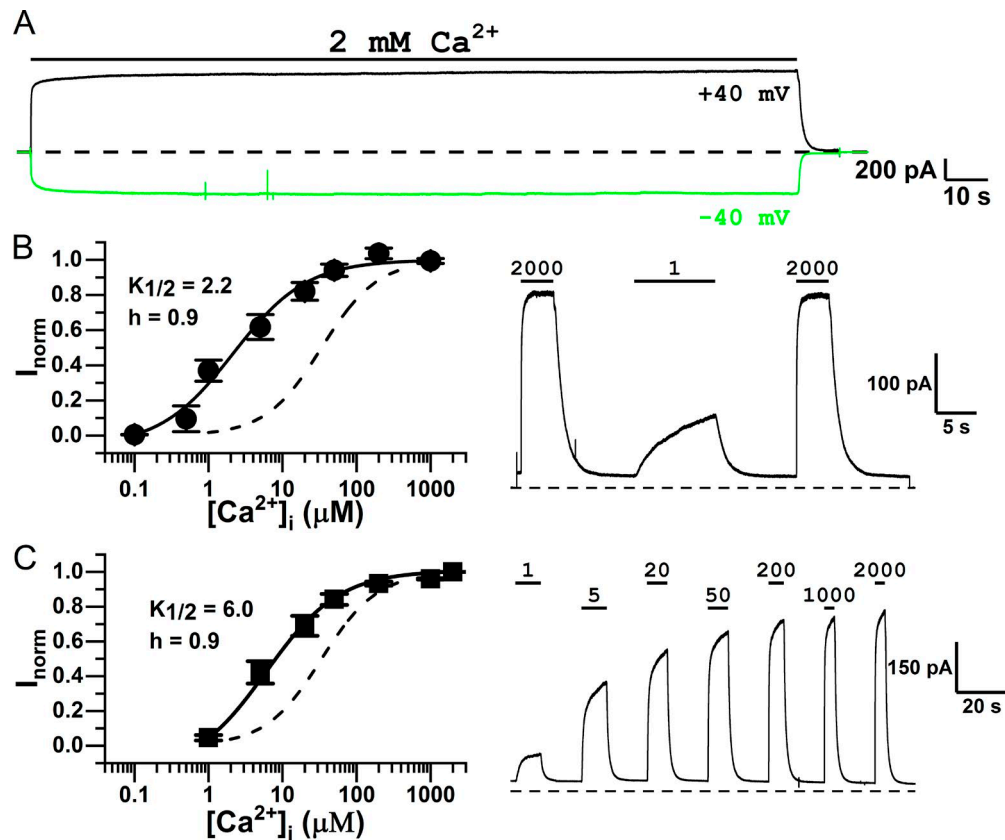


Figure 7. **Ca²⁺-dependent activation of Q559W_{16F}.** (A) Exposure of Q559W_{16F} to 2 mM [Ca²⁺]_i for 3 min (indicated by the black line on top) revealed little current rundown. (B) Examining [Ca²⁺]_i-dependent activation of Q559W_{16F} (at +40 mV) in symmetrical 140 mM [Cl⁻] using the three-pulse protocol. A representative trace of the experiment using this protocol is shown on the right. The dashed line is the zero current level. Numbers and horizontal segments above the trace represent the application of the applied [Ca²⁺]_i in μM. (C) Dose–response curve of Ca²⁺-activation of Q559W_{16F} in symmetrical 140 mM Cl⁻. Various [Ca²⁺]_i were sequentially applied as shown by the recording trace shown on the right. In B and C, all currents were normalized to that obtained with 2 mM [Ca²⁺]_i (*n* = 10–15). The dashed curve was the fitted dose–response curve of WT_{16F} shown in Fig. 4.

ative the side-chain charge, the more outwardly rectifying the I-V curve. We also adopted two other methods to change the side-chain charge: titrating the side-chain charge of a histidine residue with pH_i, and modifying the free thiol group of a cysteine residue by charged MTS reagents (Fig. 3). The results from these experiments support the idea of an electrostatic regulation of the I-V curve rectification in TMEM16A by the charge from residue 584. One somewhat surprising observation from MTS modification experiments of K584C_{16A} is that the modification rates are slow compared with the rates of modifying K519C of CLC-0. Although the position of K584_{16A} appears accessible from the intracellular aqueous solution based on the molecular structure of mouse TMEM16A, the MTS modification rates may be reduced by factors not favoring the modification. These factors, however, cannot be electrostatic in nature because both MTSES and MTSET modification rates are equally reduced. The interfering factors thus could be due to physical obstruction to reduce the accessibility of MTS reagents or due to a reduced reactivity of the thiol group of the introduced cysteine.

An electrostatic control of ion permeation in TMEM16A has recently also been reported through the analysis of I-V curve rectification in various saturation levels of the Ca²⁺-binding site. It was concluded that binding of Ca²⁺ to the binding sites, which

are located at the sidewall of the intracellular pore entrance near K584_{16A}, removes the electrostatic barrier for anion permeation exerted by those negatively charged residues forming the binding sites (Lam and Dutzler, 2018). Using a noise analysis approach, Lim et al. (2016) have previously shown that the K588Q_{16A} mutation (in the “a, c” isoform) reduces the TMEM16A channel conductance. Therefore, the mechanism of the electrostatic control from residue 584 is likely similar to that of K519 of CLC-0 in which replacing a positively charged residue with a neutral or a negatively charged residue at the intracellular pore entrance decreases the outward Cl⁻ flux (Middleton et al., 1996; Chen and Chen, 2003). On the other hand, the side-chain charge on residue 559 of TMEM16F does not show a significant correlation with the I-V curve rectification. Mutating Q559 to negatively charged residues does not change the RI of TMEM16F, while mutating Q559 to positively charged residues only slightly increases the RI. However, this small increase of the RI is not consistent with the results from the pH_i titration of Q559H_{16F}; lowering the pH_i (and thus increasing the positivity of a histidine side chain) appears to decrease the RI in Q559H_{16F} (Fig. 4). Therefore, there is no clear pattern of an electrostatic control of the I-V curve rectification by the side-chain charge of residue 559 in TMEM16F. Furthermore, we discovered that when Q559 is mutated to an aromatic

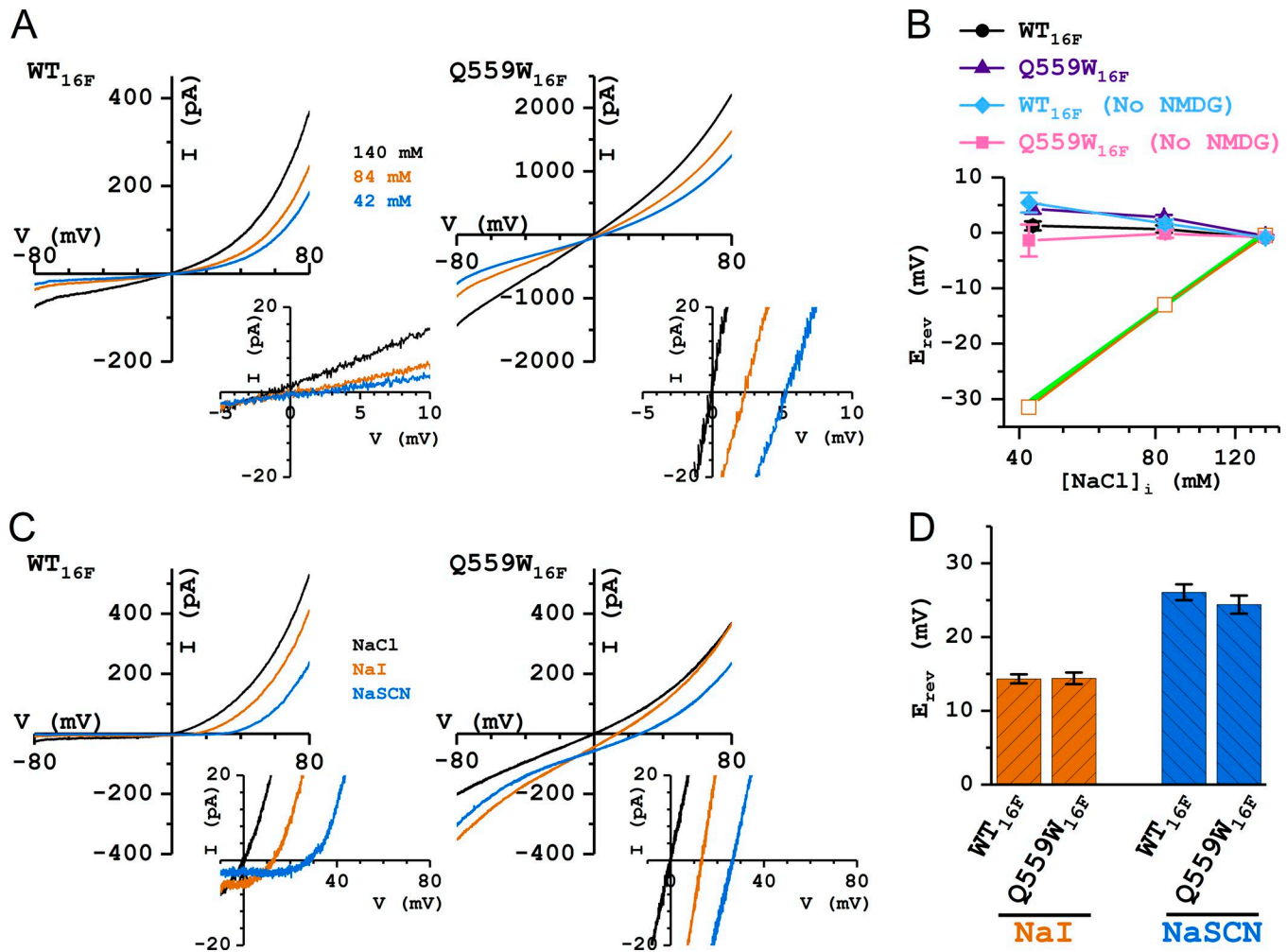


Figure 8. Comparing ion selectivity between WT_{16F} and Q559W_{16F}. All recordings were with 1 mM [Ca²⁺]_i and 140 mM [NaCl]_o. **(A)** Representative I-V curves of WT_{16F} and Q559W_{16F} in 140 mM (black), 84 mM (orange), and 42 mM (blue) [NaCl]_i. Insets show the expansion of the I-V curves near the zero current level. **(B)** Values of E_{rev} plotted against [NaCl]_i in Cl⁻ experiments of reducing [NaCl]_i with and without the replaced (NMDG)₂SO₄. Green line depicts a perfect Nernstian relation for Cl⁻. Orange squares were the mean E_{rev} of WT_{16F} in the same ionic conditions reproduced from Jeng et al. (2016). **(C)** Representative I-V curves of WT_{16F} and Q559W_{16F} in 140 mM [NaCl]_i (black), [Na]_i (orange), and [NaSCN]_i (blue). **(D)** Comparing bi-ionic potentials between WT_{16F} and Q559W_{16F}. The values of E_{rev} show no statistically significant difference between WT_{16F} and Q559W_{16F}.

amino acid, the RI significantly increases. For example, the value of the RI from 10 independent patches of Q559W_{16F} ranged from 0.24 to 0.61, in comparison with the range of 0.01–0.23 from 15 independent recordings of WT_{16F}. To our knowledge, this is the first report that mutations of TMEM16F can alter the I-V curve rectification in TMEM16F. The finding supports the idea that ion transport in TMEM16F is more likely achieved through a specific structure, possibly involving the region near Q559_{16F}, rather than a nonspecific leak. The results also support the idea that the open aqueduct in the lipid scramblase may mediate the ion transport (Yu et al., 2015; Jiang et al., 2017).

Rundown of TMEM16F alters the apparent Ca²⁺ affinity

Another unexpected finding from replacing Q559 with aromatic amino acids is that these mutants are resistant to [Ca²⁺]_i-induced current rundown. The rundown of TMEM16 proteins has been well documented (Ni et al., 2014; Yu et al., 2014a; Ye et al., 2018) and has been a hurdle in studying TMEM16 molecules. Previ-

ously, we adopted a three-pulse protocol to evaluate the apparent Ca²⁺ affinity of TMEM16A (Ni et al., 2014). This method exposes the membrane patch to testing and saturating [Ca²⁺]_i within ~10–15 s. Because the rundown of TMEM16A in such a time frame is minimal, normalizing the current induced by the test [Ca²⁺]_i to those obtained in saturating [Ca²⁺]_i provides a reasonably accurate determination of the current fraction activated by the test [Ca²⁺]_i (Ni et al., 2014). For WT_{16F}, however, the current induced by a saturating [Ca²⁺]_i (900 μM) already shows prominent rundown within several seconds (Fig. 4). Therefore, the two saturated currents before and after the test [Ca²⁺]_i in the three-pulse protocol are always significantly different, creating uncertainty on the precision of the dose–response curve. Furthermore, Ye et al. (2018) recently showed that the apparent K_{1/2} of the rundown (or desensitized) TMEM16F for Ca²⁺ (~45 μM) was significantly higher than that of the TMEM16F before rundown (~7 μM), although the rundown of TMEM16A did not affect the apparent Ca²⁺ affinity of TMEM16A (Ni et al., 2014; Dang et al., 2017). Our

finding that Q559W_{16F} shows very little rundown for several minutes provides an excellent model for the pre-rundown TMEM16F. Indeed, we show that the $K_{1/2}$ of WT_{16F} obtained from using the three-pulse protocol was $\sim 34 \mu\text{M}$ (Fig. 4 and Table 1), while the $K_{1/2}$ of Q559W_{16F} mutant and other mutants with aromatic amino acids were $\sim 2\text{--}10 \mu\text{M}$ (Fig. 7 and Table 1). This difference in the apparent $K_{1/2}$ between WT_{16F} and aromatic mutants is likely due to a decrease of Ca^{2+} affinity in the rundown WT_{16F} molecules.

The rundown-resistant mutation Q559W_{16F} did not significantly alter ion permeation of TMEM16F

Previous studies have shown that TMEM16A conducts mostly anions, while TMEM16F is less discriminating of cations from anions (Ni et al., 2014; Yu et al., 2015; Jeng et al., 2016). Measuring E_{rev} for evaluating ion permeation functions, however, is not without challenges. In recording a large current, series resistance may render the measured E_{rev} inaccurate (Yu et al., 2014b; Yu and Chen, 2015), while determining the zero current voltage for a highly rectified I-V curve could be less certain than for a more linear I-V curve. The I-V curves of TMEM16A and TMEM16F show different degrees of rectification. In saturating $[\text{Ca}^{2+}]_i$ and symmetrical 140 mM $[\text{Cl}^-]$, WT_{16A} has a linear I-V curve with an RI ($-I_{-80\text{mV}}/I_{+80\text{mV}}$) close to unity (Fig. 2), while the RI of WT_{16F} is very small, at ~ 0.05 (Fig. 5). If the inward current of WT_{16F} is further reduced (for example, by reducing the concentration of conducting ions), precise measurements of E_{rev} can be challenging (see Fig. 8 A, left panel). In mutants with an aromatic amino acid at position 559, the RI was between ~ 0.2 and 0.5, providing an I-V curve better than that of WT_{16F} for determining the zero current voltage (compare left and right panels in Fig. 8 A). Although we were more confident on the accuracy of the results measured from Q559W_{16F} than from WT_{16A}, the values of E_{rev} obtained in reduced $[\text{NaCl}]_i$ and those in $[\text{NaI}]_i$ or $[\text{NaSCN}]_i$ ended up being reasonably similar for WT_{16F} and Q559W_{16F} (Fig. 8, B and D). This indicates that the Q559W_{16F} mutations did not significantly alter the ion permeation functions of TMEM16F. The results also affirm the previous conclusion that TMEM16F does not selectively conduct Cl^- . One concern in our TMEM16F experiments of reducing $[\text{NaCl}]_i$ is that the two ions used to replace the reduced $[\text{NaCl}]_i$ (namely, NMDG⁺ and SO_4^{2-}) may permeate through TMEM16F. We chose to use (NMDG)₂SO₄ to replace the reduced $[\text{NaCl}]_i$ so that the results obtained here can be directly compared with those from our previous studies on TMEM16A (see Fig. 8 B). For the experiments of assessing anion permeation, we did not use NMDG⁺ or SO_4^{2-} , and thus the comparison of bi-anion potentials (and thus the anion selectivity) may be more direct. The results show that the anion selectivity of WT_{16F} and Q559W_{16F} still follows the type I Eisenman sequence (Eisenman, 1962): namely, $P_{\text{SCN}} > P_{\text{I}} > P_{\text{Cl}}$, similar to the previous observations in TMEM16F (Grubb et al., 2013) and in TMEM16A (Qu and Hartzell, 2000; Ni et al., 2014).

Conclusion and speculation

The I-V curve rectification presented here is more interpretable for TMEM16A than for TMEM16F. TMEM16A appears to be a classical ligand-gated anion channel. It is reasonable that K584_{16A}

exerts an electrostatic control on the outward Cl^- flux, because numerous studies have documented that a charge alteration at the pore entrance can increase or decrease the ion flux (Imoto et al., 1988; Chiamvimonvat et al., 1996; Middleton et al., 1996; Chen and Chen, 2003). In TMEM16F, however, the mechanisms underlying the change of rectification and underlying the rundown resistance in mutants with aromatic residues at position 559 remain obscure. A recent study by Ye et al. (2018) suggests that the rundown of TMEM16F may involve phospholipids. Furthermore, it has been proposed that the ion conduction pathway of TMEM16 proteins is partly composed of lipids (Whitlock and Hartzell, 2016), and molecular dynamic studies of the fungus TMEM16 protein suggest that the lipid bilayer is deformed near the aqueduct (Bethel and Grabe, 2016; Jiang et al., 2017). The existing literature thus prompts us to speculate whether the aromatic amino acids we placed at position 559 of TMEM16F may alter the interaction of phospholipids with the protein molecule. If so, are phospholipids also present in the intracellular vestibule of TMEM16A, and does the very low MTS modification rate of K584_{16A} result from obstruction by nearby phospholipids? It will require further studies to explore these speculations and to understand the role of phospholipids in the ion transport of TMEM16 molecules.

Acknowledgments

We thank Drs. Robert Fairclough, Tzyh-Chang Hwang, Takashi Kurahashi, and Hiroko Takeuchi for helpful discussions and critical reading of the manuscript.

This work was supported by National Institutes of Health grant R01GM065447 and by the Jong L. Chen Family Neuroscience Research Fund. Additionally, we thank the International Joint Research Promotion Program, Osaka University, for providing international travel support.

The authors declare no competing financial interests.

Author contributions: D.M. Nguyen and T.-Y. Chen designed research; D.M. Nguyen, L.S. Chen, W.-P. Yu, and T.-Y. Chen performed experiments; D.M. Nguyen, L.S. Chen, and T.-Y. Chen analyzed data; and D.M. Nguyen, L.S. Chen, and T.-Y. Chen wrote the paper.

Merritt C. Maduke served as editor.

Submitted: 1 October 2018

Accepted: 2 January 2019

References

- Bers, D.M., C.W. Patton, and R. Nuccitelli. 2010. Chapter 1: A practical guide to the preparation of Ca^{2+} buffers. In *Methods in Cell Biology*. M. Whitaker, editor. Academic Press. 1–26.
- Bethel, N.P., and M. Grabe. 2016. Atomistic insight into lipid translocation by a TMEM16 scramblase. *Proc. Natl. Acad. Sci. USA*. 113:14049–14054. <https://doi.org/10.1073/pnas.1607574113>
- Bevens, E.M., and P.L. Williamson. 2016. Getting to the Outer Leaflet: Physiology of Phosphatidylserine Exposure at the Plasma Membrane. *Physiol. Rev.* 96:605–645. <https://doi.org/10.1152/physrev.00020.2015>
- Brunner, J.D., N.K. Lim, S. Schenck, A. Duerst, and R. Dutzler. 2014. X-ray structure of a calcium-activated TMEM16 lipid scramblase. *Nature*. 516:207–212. <https://doi.org/10.1038/nature13984>

- Caputo, A., E. Caci, L. Ferrera, N. Pedemonte, C. Barsanti, E. Sondo, U. Pfeiffer, R. Ravazzolo, O. Zegarra-Moran, and L.J. Galiotta. 2008. TMEM16A, a membrane protein associated with calcium-dependent chloride channel activity. *Science*. 322:590–594. <https://doi.org/10.1126/science.1163518>
- Castoldi, E., P.W. Collins, P.L. Williamson, and E.M. Bevers. 2011. Compound heterozygosity for 2 novel TMEM16F mutations in a patient with Scott syndrome. *Blood*. 117:4399–4400. <https://doi.org/10.1182/blood-2011-01-332502>
- Chen, M.F., and T.Y. Chen. 2003. Side-chain charge effects and conductance determinants in the pore of ClC-0 chloride channels. *J. Gen. Physiol.* 122:133–145. <https://doi.org/10.1085/jgp.200308844>
- Chiamvimonvat, N., M.T. Pérez-García, G.F. Tomaselli, and E. Marban. 1996. Control of ion flux and selectivity by negatively charged residues in the outer mouth of rat sodium channels. *J. Physiol.* 491:51–59. <https://doi.org/10.1113/jphysiol.1996.sp021195>
- Dang, S., S. Feng, J. Tien, C.J. Peters, D. Bulkley, M. Lolicato, J. Zhao, K. Zuberbühler, W. Ye, L. Qi, et al. 2017. Cryo-EM structures of the TMEM16A calcium-activated chloride channel. *Nature*. 552:426–429. <https://doi.org/10.1038/nature25024>
- Eisenman, G. 1962. Cation selective glass electrodes and their mode of operation. *Biophys. J.* 2:259–323. [https://doi.org/10.1016/S0006-3495\(62\)86959-8](https://doi.org/10.1016/S0006-3495(62)86959-8)
- Fallah, G., T. Romer, S. Detoro-Dassen, U. Braam, F. Markwardt, and G. Schmalzing. 2010. TMEM16A(a)/anoctamin-1 shares a homodimeric architecture with ClC chloride channels. *Mol. Cell Proteomics*. 10:M110.004697.
- Falzone, M.E., M. Malvezzi, B.C. Lee, and A. Accardi. 2018. Known structures and unknown mechanisms of TMEM16 scramblases and channels. *J. Gen. Physiol.* 150:933–947.
- Grubb, S., K.A. Poulsen, C.A. Juul, T. Kyed, T.K. Klausen, E.H. Larsen, and E.K. Hoffmann. 2013. TMEM16F (Anoctamin 6), an anion channel of delayed Ca(2+) activation. *J. Gen. Physiol.* 141:585–600. <https://doi.org/10.1085/jgp.201210861>
- Hartzell, C., I. Putzier, and J. Arreola. 2005. Calcium-activated chloride channels. *Annu. Rev. Physiol.* 67:719–758. <https://doi.org/10.1146/annurev.physiol.67.032003.154341>
- Imoto, K., C. Busch, B. Sakmann, M. Mishina, T. Konno, J. Nakai, H. Bujo, Y. Mori, K. Fukuda, and S. Numa. 1988. Rings of negatively charged amino acids determine the acetylcholine receptor channel conductance. *Nature*. 335:645–648. <https://doi.org/10.1038/335645a0>
- Jeng, G., M. Aggarwal, W.P. Yu, and T.Y. Chen. 2016. Independent activation of distinct pores in dimeric TMEM16A channels. *J. Gen. Physiol.* 148:393–404. <https://doi.org/10.1085/jgp.201611651>
- Jiang, T., K. Yu, H.C. Hartzell, and E. Tajkhorshid. 2017. Lipids and ions traverse the membrane by the same physical pathway in the nhTMEM16 scramblase. *eLife*. 6:e28671. <https://doi.org/10.7554/eLife.28671>
- Kuruma, A., and H.C. Hartzell. 2000. Bimodal control of a Ca(2+)-activated Cl(-) channel by different Ca(2+) signals. *J. Gen. Physiol.* 115:59–80. <https://doi.org/10.1085/jgp.115.1.59>
- Lam, A.K., and R. Dutzler. 2018. Calcium-dependent electrostatic control of anion access to the pore of the calcium-activated chloride channel TMEM16A. *eLife*. 7:e39122. <https://doi.org/10.7554/eLife.39122>
- Lim, N.K., A.K. Lam, and R. Dutzler. 2016. Independent activation of ion conduction pores in the double-barreled calcium-activated chloride channel TMEM16A. *J. Gen. Physiol.* 148:375–392. <https://doi.org/10.1085/jgp.201611650>
- Lin, C.W., and T.Y. Chen. 2003. Probing the pore of ClC-0 by substituted cysteine accessibility method using methane thiosulfonate reagents. *J. Gen. Physiol.* 122:147–159. <https://doi.org/10.1085/jgp.200308845>
- Malvezzi, M., K.K. Andra, K. Pandey, B.C. Lee, M.E. Falzone, A. Brown, R. Iqbal, A.K. Menon, and A. Accardi. 2018. Out-of-the-groove transport of lipids by TMEM16 and GPCR scramblases. *Proc. Natl. Acad. Sci. USA*. 115:E7033–E7042. <https://doi.org/10.1073/pnas.1806721115>
- Middleton, R.E., D.J. Pheasant, and C. Miller. 1996. Homodimeric architecture of a ClC-type chloride ion channel. *Nature*. 383:337–340. <https://doi.org/10.1038/383337a0>
- Ni, Y.L., A.S. Kuan, and T.Y. Chen. 2014. Activation and inhibition of TMEM16A calcium-activated chloride channels. *PLoS One*. 9:e86734. <https://doi.org/10.1371/journal.pone.0086734>
- Paulino, C., V. Kalienkova, A.K.M. Lam, Y. Neldner, and R. Dutzler. 2017a. Activation mechanism of the calcium-activated chloride channel TMEM16A revealed by cryo-EM. *Nature*. 552:421–425. <https://doi.org/10.1038/nature24652>
- Paulino, C., Y. Neldner, A.K. Lam, V. Kalienkova, J.D. Brunner, S. Schenck, and R. Dutzler. 2017b. Structural basis for anion conduction in the calcium-activated chloride channel TMEM16A. *eLife*. 6:e26232. <https://doi.org/10.7554/eLife.26232>
- Qu, Z., and H.C. Hartzell. 2000. Anion permeation in Ca(2+)-activated Cl(-) channels. *J. Gen. Physiol.* 116:825–844. <https://doi.org/10.1085/jgp.116.6.825>
- Schroeder, B.C., T. Cheng, Y.N. Jan, and L.Y. Jan. 2008. Expression cloning of TMEM16A as a calcium-activated chloride channel subunit. *Cell*. 134:1019–1029. <https://doi.org/10.1016/j.cell.2008.09.003>
- Scudieri, P., E. Caci, A. Venturini, E. Sondo, G. Pianigiani, C. Marchetti, R. Ravazzolo, F. Pagani, and L.J. Galiotta. 2015. Ion channel and lipid scramblase activity associated with expression of TMEM16F/ANO6 isoforms. *J. Physiol.* 593:3829–3848. <https://doi.org/10.1113/JP270691>
- Sheridan, J.T., E.N. Worthington, K. Yu, S.E. Gabriel, H.C. Hartzell, and R. Tarran. 2011. Characterization of the oligomeric structure of the Ca(2+)-activated Cl- channel Anol1/TMEM16A. *J. Biol. Chem.* 286:1381–1388. <https://doi.org/10.1074/jbc.M110.174847>
- Shimizu, T., T. Iehara, K. Sato, T. Fujii, H. Sakai, and Y. Okada. 2013. TMEM16F is a component of a Ca2+-activated Cl- channel but not a volume-sensitive outwardly rectifying Cl- channel. *Am. J. Physiol. Cell Physiol.* 304:C748–C759. <https://doi.org/10.1152/ajpcell.00228.2012>
- Stauffer, D.A., and A. Karlin. 1994. Electrostatic potential of the acetylcholine binding sites in the nicotinic receptor probed by reactions of binding-site cysteines with charged methanethiosulfonates. *Biochemistry*. 33:6840–6849. <https://doi.org/10.1021/bi00188a013>
- Stephan, A.B., E.Y. Shum, S. Hirsh, K.D. Cygnar, J. Reiser, and H. Zhao. 2009. ANO2 is the ciliary calcium-activated chloride channel that may mediate olfactory amplification. *Proc. Natl. Acad. Sci. USA*. 106:11776–11781. <https://doi.org/10.1073/pnas.0903304106>
- Stöhr, H., J.B. Heisig, P.M. Benz, S. Schöberl, V.M. Milenkovic, O. Strauss, W.M. Aartsen, J. Wijnholds, B.H. Weber, and H.L. Schulz. 2009. TMEM16B, a novel protein with calcium-dependent chloride channel activity, associates with a presynaptic protein complex in photoreceptor terminals. *J. Neurosci.* 29:6809–6818. <https://doi.org/10.1523/JNEUROSCI.5546-08.2009>
- Suzuki, J., M. Umeda, P.J. Sims, and S. Nagata. 2010. Calcium-dependent phospholipid scrambling by TMEM16F. *Nature*. 468:834–838. <https://doi.org/10.1038/nature09583>
- Suzuki, J., T. Fujii, T. Imao, K. Ishihara, H. Kuba, and S. Nagata. 2013. Calcium-dependent phospholipid scrambling activity of TMEM16 protein family members. *J. Biol. Chem.* 288:13305–13316. <https://doi.org/10.1074/jbc.M113.457937>
- Tien, J., H.Y. Lee, D.L. Minor Jr., Y.N. Jan, and L.Y. Jan. 2013. Identification of a dimerization domain in the TMEM16A calcium-activated chloride channel (CaCC). *Proc. Natl. Acad. Sci. USA*. 110:6352–6357. <https://doi.org/10.1073/pnas.1303672110>
- Tien, J., C.J. Peters, X.M. Wong, T. Cheng, Y.N. Jan, L.Y. Jan, and H. Yang. 2014. A comprehensive search for calcium binding sites critical for TMEM16A calcium-activated chloride channel activity. *eLife*. 3. <https://doi.org/10.7554/eLife.02772>
- Whitlock, J.M., and H.C. Hartzell. 2016. A Pore Idea: the ion conduction pathway of TMEM16/ANO proteins is composed partly of lipid. *Pflügers Arch.* 468:455–473. <https://doi.org/10.1007/s00424-015-1777-2>
- Whitlock, J.M., and H.C. Hartzell. 2017. Anoctamins/TMEM16 Proteins: Chloride Channels Flirting with Lipids and Extracellular Vesicles. *Annu. Rev. Physiol.* 79:119–143. <https://doi.org/10.1146/annurev-physiol-022516-034031>
- Yang, H., A. Kim, T. David, D. Palmer, T. Jin, J. Tien, F. Huang, T. Cheng, S.R. Coughlin, Y.N. Jan, and L.Y. Jan. 2012. TMEM16F forms a Ca2+-activated cation channel required for lipid scrambling in platelets during blood coagulation. *Cell*. 151:111–122. <https://doi.org/10.1016/j.cell.2012.07.036>
- Yang, Y.D., H. Cho, J.Y. Koo, M.H. Tak, Y. Cho, W.S. Shim, S.P. Park, J. Lee, B. Lee, B.M. Kim, et al. 2008. TMEM16A confers receptor-activated calcium-dependent chloride conductance. *Nature*. 455:1210–1215. <https://doi.org/10.1038/nature07313>
- Ye, W., T.W. Han, L.M. Nassar, M. Zubia, Y.N. Jan, and L.Y. Jan. 2018. Phosphatidylinositol-(4, 5)-bisphosphate regulates calcium gating of small-conductance cation channel TMEM16F. *Proc. Natl. Acad. Sci. USA*. 115:E1667–E1674. <https://doi.org/10.1073/pnas.1718728115>
- Yu, Y., and T.Y. Chen. 2015. Purified human brain calmodulin does not alter the bicarbonate permeability of the ANO1/TMEM16A channel. *J. Gen. Physiol.* 145:79–81. <https://doi.org/10.1085/jgp.201411294>
- Yu, K., C. Duran, Z. Qu, Y.Y. Cui, and H.C. Hartzell. 2012. Explaining calcium-dependent gating of anoctamin-1 chloride channels requires a revised topology. *Circ. Res.* 110:990–999. <https://doi.org/10.1161/CIRCRESAHA.112.264440>

- Yu, K., J. Zhu, Z. Qu, Y.Y. Cui, and H.C. Hartzell. 2014a. Activation of the Anol1 (TMEM16A) chloride channel by calcium is not mediated by calmodulin. *J. Gen. Physiol.* 143:253–267. <https://doi.org/10.1085/jgp.201311047>
- Yu, K., J.M. Whitlock, K. Lee, E.A. Ortlund, Y.Y. Cui, and H.C. Hartzell. 2015. Identification of a lipid scrambling domain in ANO6/TMEM16F. *eLife*. 4:e06901. <https://doi.org/10.7554/eLife.06901>
- Yu, Y., A.S. Kuan, and T.Y. Chen. 2014b. Calcium-calmodulin does not alter the anion permeability of the mouse TMEM16A calcium-activated chloride channel. *J. Gen. Physiol.* 144:115–124. <https://doi.org/10.1085/jgp.201411179>
- Zhang, X.D., and T.Y. Chen. 2009. Amphiphilic blockers punch through a mutant CLC-0 pore. *J. Gen. Physiol.* 133:59–68. <https://doi.org/10.1085/jgp.200810005>